Small Structures

small structures

www.small-structures.com

RESEARCH ARTICLE OPEN ACCESS

Precise Capture of Membrane Proteins Using DNA-Origami-Constrained Nanodiscs

Piotr Stepien[1,2] | Gerrit Wilkens[1,3,4] | Sylwia Swiatek[1] | Manuel Yusef Robles[1] | Anna Swietlikowska[1,5] | Sarah Hutchings[2] | Dmitry Ghilarov[1,6] | Jonathan G. Heddle[1,2]

[1]Malopolska Centre of Biotechnology, Jagiellonian University, Krakow, Poland | [2]Centre for Programmable Biological Matter, Department of Biosciences, Durham University, Durham, UK | [3]Postgraduate School of Molecular Medicine, Warsaw, Poland | [4]Centre de Biologie Structurale, CNRS, INSERM, Université de Montpellier, Montpellier, France | [5]Laboratory of Chemical Biology, Department of Biomedical Engineering and Institute for Complex Molecular Systems, Eindhoven University of Technology, Eindhoven, The Netherlands | [6]Department of Biochemistry, University of Oxford, Oxford, UK

Correspondence: Piotr Stepien (piotr.stepien@durham.ac.uk) | Jonathan G. Heddle (jonathan.g.heddle@durham.ac.uk)

Received: 29 September 2025 | **Revised:** 12 March 2026 | **Accepted:** 19 March 2026

Keywords: biological nanorobots | DNA origami | membrane proteins | nanodiscs

ABSTRACT

Membrane proteins play a key role as cellular gatekeepers, regulating the flow of information and material across lipid membranes. Engineered, membrane-bound biological nanosystems similarly require membrane proteins along with the molecular tools capable of placing individual copies of them with nanometer-scale precision. To address this, we have developed DNA-origami-constrained nanodiscs (DOC-NDs) by integrating nanodisc technology with DNA origami. DOC-NDs allow for efficient capture of membrane protein-loaded nanodiscs inside a 46 nm DNA origami ring while maintaining unobstructed physical access to the captured protein. Here, we present efficient methods for the preparation of cargo-loaded DNA-modified capture-ready nanodiscs and show their capture by DOC-NDs using atomic force microscopy (AFM) and cryogenic electron microscopy (cryo-EM). Additionally, we show a proof-of-concept advanced DOC-ND variant that provides a first step toward control of the orientation of the membrane protein relative to the DNA origami ring. We envisage that DOC-NDs will support the development of next-generation systems where membrane proteins can not only be precisely positioned for biochemical and structural analysis but also delivered to target lipid bilayers to tailor permeability of synthetic cells and their compartments.

1 | Introduction

Membrane proteins (MPs) are among the most important constituents of living organisms: The DNA encoding them is estimated to comprise 20%–30% of the genomes of both prokaryotes and eukaryotes [1–4]. As MPs govern the transport of material and transduction of signals across cellular membranes, they are privileged drug targets, with around 60% of small molecule pharmaco phores specifically targeting them [5, 6].

Beyond their biological significance, MPs are one of the most important building blocks for artificial systems in synthetic biology applications, where they can be used in roles analogous to those in nature, i.e., gating of materials and information across lipid membranes [7]. The precise control of lipid and protein composition of membranes allows preparation of systems with selective permeability, which can be used as tools for a deeper understanding of natural systems [8] as well as for numerous biotechnological applications [9].

One of the most important tools for handling MPs is nanodiscs [10] (NDs)—nanometer-sized patches of lipid bilayers stabilized at their circumference by a dimer of membrane scaffold proteins (MSPs). Their lipid content and size can be precisely controlled, consequently allowing control of the oligomeric state of the incorporated MPs [11]. In recent years, the ability of NDs to render MPs soluble in a detergent-free aqueous environment has proved invaluable for biochemical and structural studies [12, 13], especially cryogenic electron microscopy (cryo-EM) [14–20]. ND

technology is constantly being updated to improve spectral properties [21], stability [22], and charge [21, 23]. However, it is the merger of NDs with the modular DNA nanotechnology, specifically with scaffolded DNA origami [24, 25], which can provide an extra layer of control over stabilized MPs and ease further functionalisation [26]. This is due to the unique addressability of each strand in the DNA origami designs, allowing for the spatial arrangement of biomolecules at defined stoichiometries [27].

While NDs have been previously interfaced with DNA origami to create spatially arranged arrays of NDs [28], and as a tool to build DNA origami-encircled planar lipid bilayers [29], these approaches do not enable the precise capture, geometric confinement, or controlled orientation of individual NDs carrying individual MPs. Existing strategies typically rely on single-point tethering, which allows substantial positional and rotational freedom, and they do not provide a means to deterministically position single MPs within a defined nanoscale cavity. As a result, an origami-based technique for precise capture and spatial constraining of individual NDs carrying MPs has not yet been developed. Such a system would enable fine spatial control of MPs to place them where and when required for bottom-up construction of artificial systems, imaging, or therapeutic effects.

To achieve such fine control, we developed DNA origami-constrained NDs (DOC-NDs), a method to efficiently sequester individual MP-loaded NDs inside a single DNA origami, and demonstrated proof-of-concept of a ND-capturing mechanism with potential for control of the relative orientation of the MP inside a DNA origami (Figure 1).

2 | Results

2.1 | Preparation of DOC-NDs for Precise ND Placement

To create our DOC-NDs, we first equipped the NDs with "foundational" ssDNAs. These are DNA strands designed to bind to complementary strands lining the inner circumference of the DNA ring. Using a previously prepared molecular dynamics model of the MSP ND [30], we selected two solvent-exposed residues (Ser 22 and Ala 157) in MSP1E3D1 protein expected to face in roughly four different directions, approximating the four cardinal points in the MSP dimer found in the assembled NDs, and mutated them to cysteines (Figure 2A; the protein has no native cysteines). MSP1E3D1$^{S22C,\ A157C}$ was purified and used to prepare NDs. After ND assembly, the introduced cysteines were coupled with maleimide-ssDNA (Figure 2B), and the unreacted ssDNA was removed using size exclusion chromatography (Fig. S1A,B). The yield was estimated based on densitometric

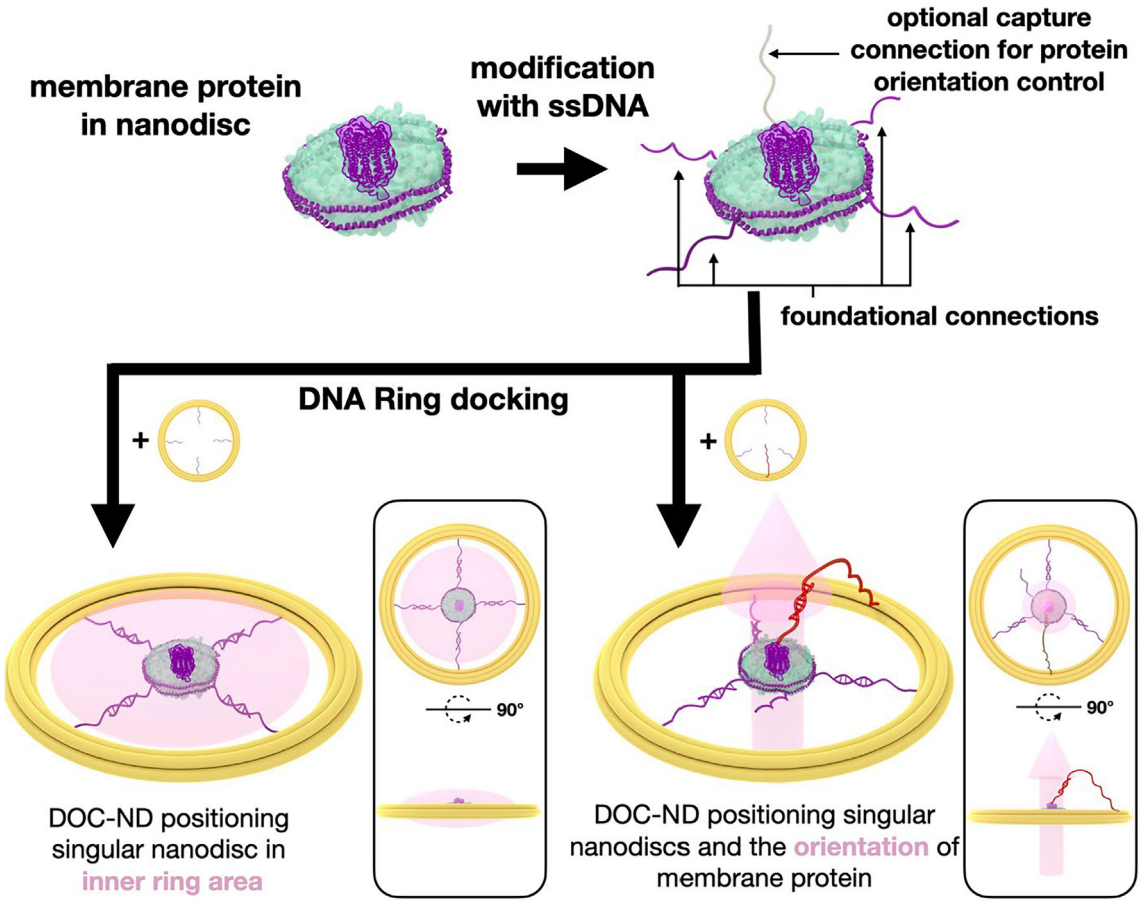

FIGURE 1 | Design of DOC-NDs for capture of MP-containing NDs. The NDs carrying MP are equipped with four "foundational" ssDNA extensions by modification of the stabilizing, belt-like MSP dimer. Additionally, the MP itself can be equipped with an optional "capture" ssDNA for more advanced control. The foundational connections can be used to precisely position the NDs within the inner area of the DNA origami ring carrying complementary DNA (bottom left; confinement area highlighted). The inclusion of the optional capture strand on the MP enables finer manipulation by enforcing MP orientation relative to DNA ring (bottom right, extracellular part of protein facing up from the plane of the ring highlighted with an arrow).

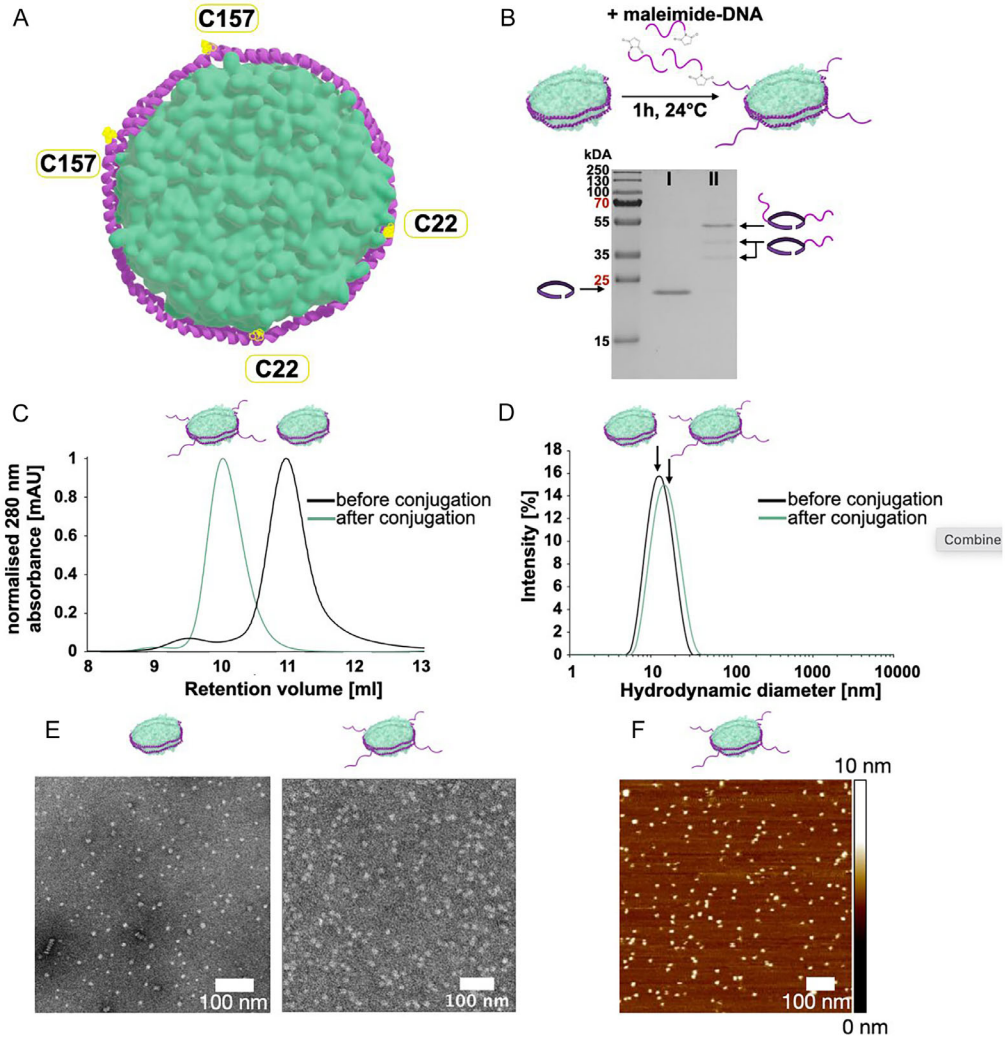

FIGURE 2 | Modification of NDs with DNA foundational strands. (A) Surface (lipid) and cartoon (protein) representation of a MSP1E3D1$^{S22C\ A157C}$ ND showing the layout of residues changed to cysteines for the attachment of ssDNA to the NDs. (B) Scheme of maleimide-DNA conjugation to cysteine residues in preformed NDs above a Coomassie blue-stained SDS-PAGE gel showing the MSP1E3D1$^{S22C\ A157C}$ NDs prior to reaction (lane I) and post-reaction with maleimide-DNA (lane II). The high molecular weight band corresponds to MSP1E3D1$^{S22C\ A157C}$ with two DNA strands attached, and the two faster migrating bands correspond to proteins with a single DNA strand attached (see Supporting Notes). Protein molecular weight marker bands (top to bottom) 250, 130, 100, 70, 55, 35, 25 and 15 kDa. Cartoons depict the MSP1E3D1$^{S22C\ A157C}$ proteins as belts with and without the DNA strands present. The gel shown is also shown in Fig. S1. (C) SEC, (D) DLS, and (E) NS-TEM data for NDs pre- and postreaction. (F) AFM micrographs showing the postreaction NDs.

analysis of Coomassie-stained SDS-PAGE gels (Fig. S1C,D), showing that ∼83% of NDs have three or more DNA strands attached to them (Figure 2B, Table S1). A comparison of size exclusion chromatogram (SEC) profiles of pre- and postreaction NDs confirmed that virtually all NDs were modified with DNA, as no NDs in the postreaction trace were present at the elution volume characteristic for unmodified ND. (Figure 2C) The dynamic light scattering (DLS) and negative stain transmission electron microscopy (NS-TEM) and atomic force microscopy (AFM) data showed that ssDNA-NDs retained compact and well-defined morphology; however, the resolution of the methods did not allow visualization of attached, flexible ssDNA (Figure 2D,E,F).

To capture the prepared DNA-modified NDs inside the DNA origami rings, we have adapted a 46 nm diameter, ring-shaped six-helix bundle DNA origami [31] so that an individual ND can be constrained within the plane encircled by the ring. The large open cavity was chosen to allow facile access to the ND after capture and flexibility of connection for potential downstream applications. The DNA origami design includes four complementary, identical, and equally spaced "docking" strands used for ND attachment via foundational strands introduced into the NDs (Figure 3A).

The four strands provide a degree of redundancy as only three points of connection are required to place the NDs in the plane of DNA ring (i.e., the disc circumscribed by the ring) and to prevent ND rotation. This engineered redundancy was expected to mitigate the need for ideal modification of ND with ssDNA and, thus, to improve the overall yield of the procedure, making it practicable and scalable. The connections are spaced every $\pi/2$ rad on the inner circumference of the DNA ring and contain a polythymidine linker whose length was optimized to ensure optimal ND placement (Figure 3B). As a starting point, we tested strands containing 14 thymidine repeats, which were expected to

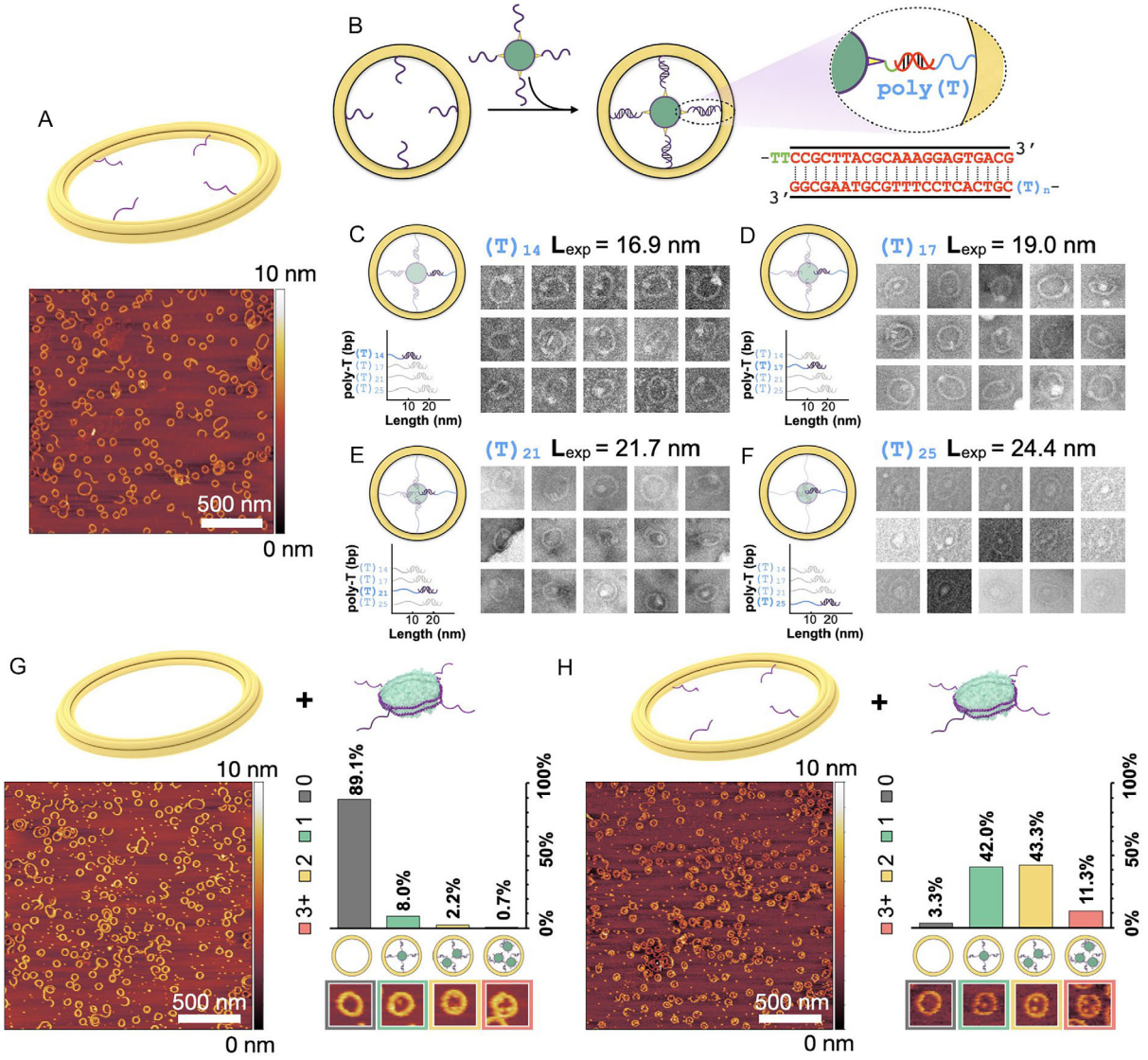

FIGURE 3 | Specific capture of NDs within the DOC-NDs. (A) A model of a DNA ring (colored yellow) containing four foundational capture strands (colored purple) (top) and an AFM micrograph of prepared structures (bottom). (B) To achieve assembly, a ND modified with four ssDNA strands is docked by complementary strands on the DNA ring. The strands attached to the NDs are composed of a linker region (green) and a hybridization region (red). The strands on the DNA ring contain a complementary hybridization sequence (red) and an adjustable polythymidine linker (blue). (C–F) Schematic depictions of different linkers and their expected theoretical lengths (L_{exp}) along with representative micrographs of DNA rings with bound ND imaged using NS-TEM (box size 100x100 nm) for polythymidine linkers (C) $T = 14$, (D) $T = 17$, (E) $T = 21$, and (F) $T = 25$. An AFM micrograph of DOC-NDs without (G) or with (H) inclusion of capture strands in DNA rings mixed with DNA-NDs along with bar graphs showing the distribution of imaged particles and exemplary particles for each category (box size 100x100 nm). The same AFM images shown in panels (G) and (H) are also presented in Figures S2 and S3 with additional details illustrating selection of rings for counting.

be ~16.9 nm (L_{exp}) in length assuming length of a single unit of $L_{dsDNA} = 0.34$ nm [32] and $L_{ssDNA} = 0.676$ nm [33]. This connection length theoretically provides an optimal fit with the DNA fully extended and the ND placed precisely in the center of the DNA ring. In practice, while NDs attached to the DNA ring were observed using NS-TEM, the majority were somewhat off-center or the DNA ring had an elongated shape, suggesting mechanical tension arising from the connections being of insufficient length. The length of the poly-T linker was subsequently increased to 17, 21, and finally to 25 bases, with every increment improving the placement of NDs and the final value of 25 providing the desired result with mostly central positioning of NDs (Figure 3C–F). The linker length is also expected to provide the NDs with a modest degree of freedom along the *z*-axis, a feature advantageous for future applications as discussed in the Discussion.

Using optimized connection length, we tested the efficiency of ND capture by preparing DNA rings with and without ND docking foundational strands and mixing them with excess NDs (Figure 3G,H). This allowed us to control for the NDs which may be observed within the circumference of the DNA ring during imaging, but which may not be specifically attached. AFM visualization of DOC-NDs without the foundational strands present showed that only ~11% of the rings contained NDs. Upon

introduction of the foundational strands, ~97% of rings contained NDs with ~42% containing individual NDs and the rest having two or more (Fig. S2 and S3), showing that the capture strictly depends on the presence of foundational strands. Because NDs were added in excess (ND:DOC = 3:1), a substantial fraction remained unbound and based on AFM counting and the observed loading distribution, this fraction is estimated to be approximately 46%–52%.

Having established that the system is capable of selectively capturing DNA-modified NDs, we prepared DOC-NDs containing MPs and carried out more detailed imaging. We prepared NDs containing monomeric bacteriorhodopsin (bR) and modified them postassembly as described above (Figure 4A–C and S4, Table S2). To better assess placement of NDs within the DNA ring, the amount of DNA rings containing NDs (loading efficiency), and the amount of NDs per DNA ring (loading state), we employed cryo-EM. Because a substantial fraction of NDs remains unbound in the initial assembly mixture, these were removed prior to imaging by ultracentrifugation in a glucose density gradient (Fig. S5 and S6), and the sample was imaged in single-particle mode on ultrathin carbon-covered grids.

Based on a visual inspection of 2044 DNA rings, 83.5% contained NDs and within those, 64.1% were loaded with a single ND. For DNA rings loaded with more than one ND, the majority (>50%)

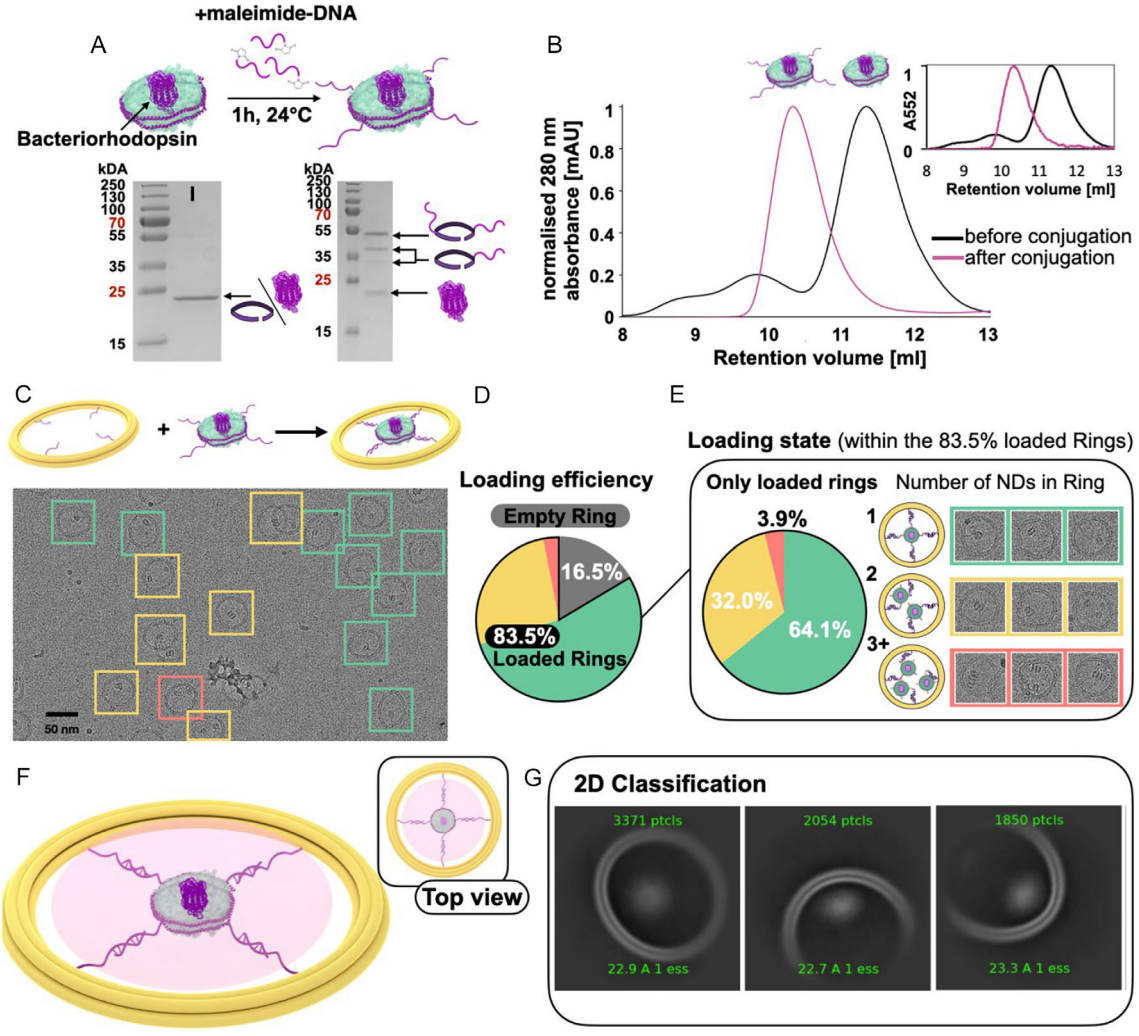

FIGURE 4 | Efficiency of capture of MP-bearing NDs in DOC-NDs. (A) A scheme of maleimide-DNA conjugation to cysteine residues in preformed NDs and Coomassie blue-stained SDS-PAGE gels showing the MSP1E3D1$^{S22C\ A157C}$ bR-containing NDs before reaction (left lane) and post reaction with maleimide-DNA (right lane). Postreaction the highest mass corresponds to MSP1E3D1$^{S22C\ A157C}$ with 2 DNA strands attached and the two lower mass bands correspond to proteins with a single DNA strand attached either C22 or C157. The lowest mass bands of unmodified MSP1E3D1$^{S22C\ A157C}$ and bR overlap due to similar molecular mass. Cartoons depict the MSP1E3D1$^{S22C\ A157C}$ proteins as belts and bR with and without the DNA strands present. The same gels are also presented in Fig. S4. (B) SEC data for NDs pre- and postreaction. The inset shows absorbance at 552 nm, confirming the presence of bR in NDs. (C) Schematic depiction of docking of bR-containing ND in DNA ring. An exemplary cryo-EM micrograph showing bR-NDs captured with the DNA ring with boxes showing particles classified within the visual analysis. (D) Efficiency of loading of NDs into DNA ring and (E) the distribution of the number of NDs captured by individual rings. Data based on visual analysis of motion-corrected cryo-EM DNA micrographs (total of 2044 particles); exemplary particles for every loading state are shown (box size: 70x70 nm). (F) Model of the idealized DOC-ND with the captured ND with area to which ND is constrained highlighted in pink. Inset: top view of the assembly. (G) 2D class averages of particles containing DNA ring acquired by cryo-EM showing successful capture of NDs (box size: 70x70 nm). These images are also included in Fig. S8 as part of a larger set illustrative of obtained 2D classes.

involved clear stacking [34] of NDs (Figures 4D–F and S7 and S8). This stacking was already present in unbound NDs prior to ultracentrifugation (Fig. S6), and as such, it is not a consequence of the interaction with the DNA origami in our system.

Importantly, virtually all the imaged NDs were constrained within the interior of the DNA ring and aligned well with the designed confinement area in this foundational DOC-ND variant, achieving our initial goal of a system for efficient capture and sequestration of NDs in DOC-NDs. Figure 4F shows the idealized fully engaged configuration; in practice, the spread in Figure 4G likely arises from linker flexibility and variation in the number of engaged tethers, without compromising confinement within the ring. This is best visualized by inspecting the 2D class averages of DNA rings where median positions of constrained NDs can be seen (Figure 4G) with 46% centrally positioned, less than 4 nm off-center, and the remaining particles more offset but still enclosed by the ring and positioned less than 12 nm off-center. Notably, when imaging the origami rings with cryo-EM, no damaged rings were visible (Fig. S7), implying that the broken and open structures observed previously using AFM were artifacts of the imaging method, while the lack of large "ring-like" structures, most likely being the origami dimers, were removed using ultracentrifugation purification.

2.2 | Preparation of DOC-NDs for Orientation Control of MPs

With the foundational DOC-ND system for efficient capture and placement of NDs within the DNA ring established, we next attempted to expand the functionality of the system. Crucially, we aimed to create a design that allows for an increased yield of single ND capture precisely in the center of the DNA rings and for the possibility to control MP orientation relative to the plane of the origami.

The first adjustment was to alter the number of docking foundational strand connectors within the DNA ring from 4 to 3 (Figure 5A), spaced every $2\pi/3$ rad on the DNA ring's inner circumference. The aim was to reduce the likelihood of individual NDs becoming trapped off-center due to the specific order in which DNA strands are annealed (Fig. S9). Additionally, to maximize the loading of individual NDs, we introduced a new connection into our setup—for the direct tethering of the MP inside the captured ND to the DNA ring via the ND "capture" strand (Figure 5A). This, together with the sequential docking methodology (described below and in Figure 5B,C), should have, in principle, allowed for the capture of NDs in an ideal 1:1 stoichiometric ratio within DOC-ND. Moreover, as the new connection is placed directly on the MP and is positioned asymmetrically, off-plane relative to the DNA origami ring, it had a potential to control the orientation of the MP in respect to plane of the DNA origami (Figure 5D).

To assemble this DOC-NDs variant, we introduced a unique cysteine residue on the N-terminus of bR (originally cysteine-free), coupled it with 23-bp maleimide DNA (Supporting Information methods), and, using affinity and ion exchange chromatography, removed the free DNA and unmodified protein (Fig. S10). The purified DNA-bR was subsequently incorporated into NDs, and the loaded NDs were modified with DNA and purified (Figures 5B and S11). The spectral properties of retinal inside bR remained unchanged after all the preparation steps, suggesting that the chromophore, and by extension, protein structure, remained intact (Fig. S12).

Next, we designed and implemented the stepwise docking protocol (Figure 5C), where the foundational strands on the DNA ring are initially occupied by "blocking" strands, thus preventing direct attachment (docking) of NDs in the DOC-NDs. As a result, upon mixing, the NDs are expected to initially bind to DNA ring only via the hybridization of the capture strand present on the MP. This, together with the fact that NDs carry individual copies of bR, means that at most one ND is expected to be bound to one DNA ring via hybridization of the capture strand and bR-DNA. Following this, the excess of unbound NDs can be removed using ultracentrifugation and the foundational strands can be unlocked using toehold-mediated strand displacement (Fig. S13 and S14) to allow for docking of the NDs captured via the MP-bound tether inside the plane of the DNA ring. The efficiencies of the individual steps were estimated using strand-only reactions (i.e., without NDs or DOCs) (Fig. S15). Under these conditions, the blocking strand occludes ~100% of the docking strands. In the presence of the ND strand but without release strand, ~91% of ND strands remain in the blocked (non-DOC-binding) state. Upon addition of the release strand, ~46% of ND strands are shifted into the simulated DOC-bound state, ~12% remain free, and ~41% form an ND–release complex. It is important to note that this strand-only assay represents a conservative benchmark: in the assembled DOC-ND system, multiple DNA handles per ND are expected to increase effective local concentration and multivalency, thereby disfavoring the ND-release side complex and improving productive docking relative to the minimal strand-only case.

We were not able to generate a sufficient number of particles for single particle cryo-EM analysis, as we could not reach required concentrations and the majority (>90%) of particles imaged were damaged (Fig. S16), primarily due to deformation/opening of the DNA origami ring rather than loss of ND capture. However, using cryoelectron tomography (cryo-ET), we were able to visualize the intact, complete individual assemblies in detail. The imaged particles contained four distinct DNA connections, clearly visible in the z-axis slices of the acquired tomograms (Figure 5E). Additionally, all the connections, as designed (Figure 5D, inset), were arranged in a distinctive pattern reminiscent of a "peace sign". We were able to ascribe the capture strand to the appropriate density placed between two of the three docking connections. The capture strand is expected to be positioned off the plane of DNA origami (Figure 5A), and, indeed, it is found in the most extreme slices of the tomographs. In addition, the reach distribution estimated for the orientation-defining tether (Supporting Note 3; Fig. S17) indicates that the extended configurations required for a complete "flip" are strongly disfavored under equilibrium conditions. Moreover, the visualized ND are coplanar with the origami ring and while we do not resolve individual strands in the 3D density representation at the current resolution, side views reveal ND-associated density extending out of the ring plane, consistent with the presence of an out-of-plane connection (Fig. S18). All this strongly suggests that the MP orientation relative to DNA origami is constrained.

The identified DNA connections overlaid on densities acquired from tomography are presented in Figure 5E and show the successful preparation of the advanced version of the DOC-ND system.

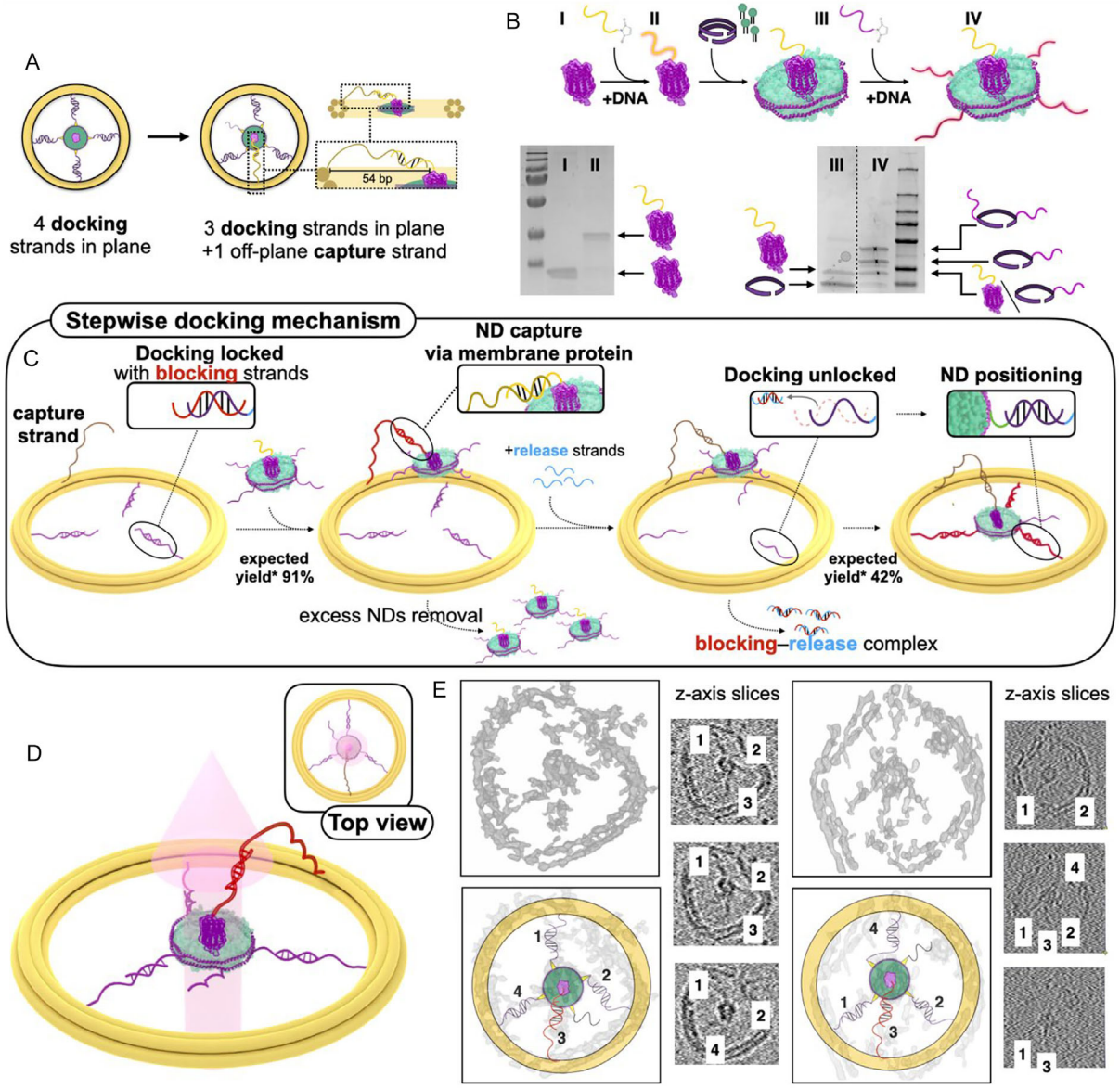

FIGURE 5 | Preparation of advanced DOC-NDs for orientationally controlled capture of MPs. (A) Adjustments made to the previous iteration of the design, including the change from four ND capture strands to three and the addition of one off-plane strand to capture and control the orientation of MPs, exemplified by bR. (B) Top: Scheme illustrating DOC-ND preparation and (bottom) the accompanying Coomassie blue-stained SDS-PAGE gels demonstrating preparation of the bR-NDs containing all the necessary DNA connections. I: the MP is modified and purified to provide II: DNA-protein used for assembly of III: NDs, which are subsequently modified with ssDNA to provide IV: "capture-ready" NDs. Cartoons depict the MSP1E3D1$^{S22C\ A157C}$ proteins as belts and bR with and without the DNA strands present. Line denotes location where gel was spliced for clarity of presentation. (C) Schematic illustrating the stepwise docking mechanism of the capture-ready NDs. The NDs are first captured via the ssDNA present on MP by the DNA rings with blocked docking foundational strands (efficiency of blocking in test strand-only experiments* was shown to be ~100%, and the efficiency of ND capture without engaging the docking strands 91%, Fig. S15). Following this, the excess NDs are removed, and the docking strands are unlocked, allowing for the placement of NDs inside the ring with controlled orientation (efficiency of this capture is estimated to be minimum of 42% as shown by strand-only tests*, Fig. S15). (D) Idealized model of an assembled advanced DOC-ND system showing the ssDNA capture (highlighted) strand forcing the orientation of MP to be approximately normal to the plane of the ring (shown with an arrow). Inset: top view of the assembly. (E) cryo-ET densities and z-slices showing the successful assembly of the designed DNA connections and capture of NDs in the center of the DNA ring. The shown individual DOC-ND assemblies were imaged from two independent preparations of advanced DOC-NDs, including independent preparations of all components (box size: 60x60 nm).

3 | Discussion

This work demonstrates how a combination of DNA nanotechnology and lipid NDs can result in a structure with the potential to capture and control individual MPs.

The foundational DOC-ND system (Figure 4) requires only modification of MSP in NDs with ssDNA.It enables efficient loading, with 64.1% of DNA origami rings capturing individual NDs carrying single MPs, each positioned within the 46 nm central cavity. The robust protocol, upon scaling up, allows for the preparation of material in quantities satisfying the requirements of single-particle cryo-EM analysis. The fraction of DOC-NDs with individually captured NDs could potentially be further

increased to ~80% by reducing ND stacking, a phenomenon linked to the presence of divalent cations [34]. This could be addressed by reducing the concentration of Mg^{2+} used during assembly to the minimal amount required for DNA origami stability [35]. Additionally, for larger MP targets, steric hindrance from their bulky soluble domains is expected to disfavor stacking [36]. Although stacking occurs only to a limited extent in our experiments, it should be minimized using the strategies described above to ensure optimal performance in cryo-EM applications. Alternatively, to increase the loading of individual NDs, DNA origamis with a smaller cavity for ND capture can be used. However, this might limit access to the MP in ND for future manipulation or imaging. Additionally, the larger cavity presented here, together with the adjustable poly-T linkers, allows for use of different sizes of NDs, from 5 to 17 nm in diameter [13, 37–39], to match the MP of interest.

In the advanced DOC-ND system (Figure 5), we have demonstrated a proof-of-concept docking methodology that enables precise capture of individual MPs and control of their orientation with respect to the DNA origami ring. Precise loading was achieved by distinct ssDNA handles attached to the MP and ND combined with stepwise capture protocol based on strand displacement. In contrast to standard strategies where molecules are functionalized with single or multiple copies of the same ssDNA [40–42] for direct hybridization, this approach resembles multihandle sequential binding used in force spectroscopy.

These data show that the sequential docking approach is a viable method for precisely placing MP-loaded NDs in DNA origami with an unprecedented degree of control, as shown in the successfully assembled advanced DOC-NDs (Figure 5E). The method should be readily transferable to other DNA origami designs. The low yield of the advanced DOC-NDs likely results from repeated heating steps during sample preparation, leading to DNA origami ring opening and damage to the DOC-ND assemblies (Fig. S14). In the future, this can be overcome by increasing ring robustness without changing its diameter or compromising the connection flexibility required for downstream applications in delivery outlined later. This can be achieved by using more thermostable DNA origami designs, for example, a 12-helix bundle ring [31] or crosslinking [43], to enable robust and scalable capture of MP-loaded ND at scale. Those will additionally prove useful in single-particle analysis, allowing a more detailed display of orientation control.

The conjugation strategy of postassembly DNA modification of NDs can be easily adapted to diverse MPs without altering existing purification and reconstitution protocols. For MPs containing surface-exposed cysteine residues, the methodology can be modified by employing alternative DNA-conjugation strategies. The cysteines in the NDs can be replaced with unnatural amino acids such as 4-azido-L-phenylalanine and reacted with DBCO (dibenzocyclooctyne)-modified DNA [44]. For MPs, a similar approach or alternative bioconjugation strategies [45–49] can be used. Regardless of the chemistry employed, the overall preparation scheme will remain unchanged.

We have developed the DOC-ND as a modular platform, which, rather than addressing a single application, offers a generalizable solution for positioning and manipulation of MP at the nanoscale. As such we hope that it can be built upon for diverse applications in MP research, imaging, and synthetic biology. Potential applications are in basic research, where the capture of MP within the DNA ring of the DOC-ND could be used for single-molecule MP studies or cryo-EM imaging of MPs. In cryo-EM, by virtue of fine control of the protein's position and DNA rings being oriented preferentially in a flat conformation in the vitreous ice, the MP in NDs can be forced into underrepresented orientations [50, 51].

While not demonstrated experimentally in this work, the DOC-ND architecture was designed with potential future

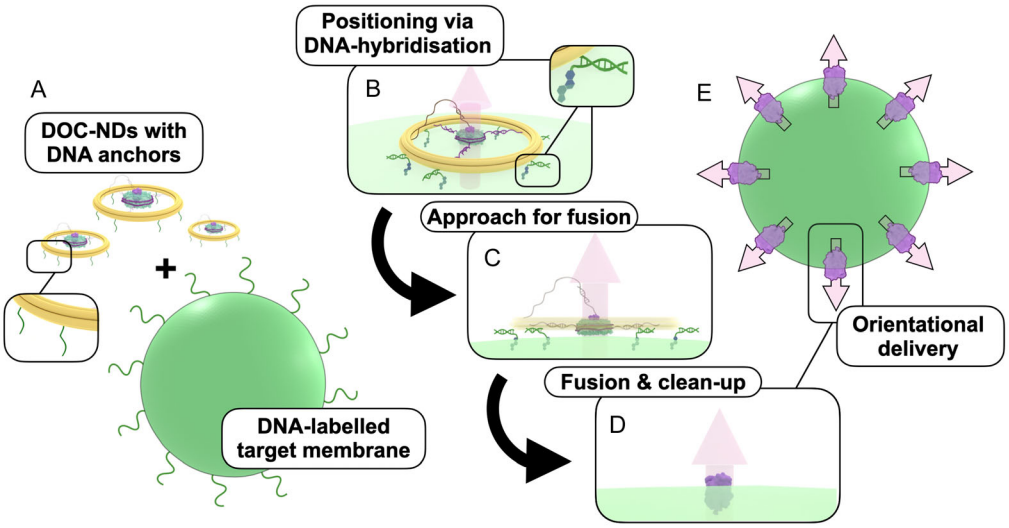

FIGURE 6 | Forward-looking perspective for possible use of DOC-NDs for controlled delivery of MPs. (A) DOC-NDs can be equipped with ssDNA strands complementary to ssDNA strands embedded in targeted membrane. (B) The DNA hybridization could position the DOC-NDs on the targeted membrane, in case of advance DOC-NDs (shown) potentially positioning the MP in the desired orientation with respect to the targeted membrane. (C) The open architecture of DOC-NDs and the flexibility of linkers may allow the ND to be in proximity of the membrane so that fusion could take place upon external triggering. (D) After fusion and removal of the DOC via, i.e., nuclease treatment or toehold-based approaches, the MP would be placed within the membrane, retaining its orientation as guided by the DOC-NDs. (E) This modality of protein delivery could in future equip the targeted membrane with MP with selected orientation, allowing for tailoring their permeability.

membrane-interfacing applications in mind. In synthetic biology, the DOC-ND system offers a foundation for the development of programmable MP delivery platforms. DNA hybridization-based docking [52] or pH-sensitive docking [53] could be, in principle, integrated into the origami to direct and position DOC-NDs on chosen ssDNA-tagged lipid membranes in a triggerable fashion (Figure 6A). This positioning can be further spatially organized using phase-separated lipid domains [54], lipid-bound DNA networks [55], and 2D supramolecular origami assemblies [56]. After this precise placement (Figure 6B), the singular MP carried in the DOC-ND might in future be transferred into the destination membrane with lipid fusion-based techniques like the recently reported nanoCRAFT—a method for rapid, on-demand ND fusion [57]. The MP delivery events would be localized to an area smaller than the inner circumference of the DNA ring, and importantly the open architecture and flexibility of connections of DOC-ND can potentially allow ND to approach the target membrane so that the fusion can take place (Figure 6C). Importantly, the enforced orientation of the ND in DOC-ND could, in principle, enable selection of the orientation of the delivered MP in the target membrane (Figure 6D) to tailor its permeability (Figure 6E). As such, the proposed devices may provide a basis for future strategies to precisely manipulate MPs to enable bottom-up construction of artificial cells in a true block-by-block fashion.

4 | Conclusions

In this work, we demonstrate the design and preparation of NDs bearing multiple ssDNA strands and two approaches for their precise placement within DNA origami constructs (DOC-NDs) using multiple attachment points. Importantly, our methodologies preserve key structural and handling advantages inherent to NDs, such as the ability to capture and stabilize individual MPs. The open architecture of the origami ring ensures that both sides of the ND and, by extension, the MP remain accessible to the solution. The ability of the prepared DOC-ND to capture individual MPs and their potential for controlling their orientation builds a foundation for developing bespoke, precise MP delivery and imaging systems.

5 | Methods

5.1 | Materials

Staple strands for DNA origami were purchased from Integrated DNA Technologies, Inc. and maleimide-modified DNA oligonucleotides were purchased from biomers.net GmbH. DMPC was purchased from NOF Japan and other compounds were purchased from Merck KGaA. All molecular cloning steps were done using 5-alpha Competent *Escherichia coli* (New England Biolabs) and all protein expression was done using BL21(DE3) Competent *E. coli* (New England Biolabs).

5.2 | Protein Expression and Purification

Plasmid for expression of MSP1E3D1 was a gift from S. Sligar [58] (Addgene plasmid no. 20 066) and was used as a template for the preparation of MSP1E3D1$^{S22C,\ A121C}$ using two rounds of site-directed mutagenesis polymerase chain reactions. In first (S22C), the primers CAGGGTTGTACCTTCAGTAAACTTCG and TCGCGAAGTTTACTGAAGGTACAACCC were used and in second (A157C) CGCTGCGTTGCGAACTGCAAGAGG and GCAGTTCGCAACGCAGCGGTTCC. For each step, the products were verified using Sanger sequencing. The MSP1E3D1$^{S22C,\ A121C}$ was purified using a standard protocol [39]. The plasmids for bacteriorhodopsin (*Halobacterium salinarum*) with and without N-terminal cysteine (C138) were constructed and the proteins were purified as described previously [57]. For the preparation of the foundational system, the cysteine-free bacteriorhodopsin was used, and for the orientation-controlled variant, a DNA-modified bR (C138; near the N-terminus) was used.

5.3 | bR Conjugation with DNA

bR(C138) stock solution was reduced by mixing 1:1 (vol:vol) with 50 mM NaH_2PO_4, 250 mM NaCl, 4 mM TCEP, 2 mM EDTA, pH 8, followed by 1 h incubation at room temperature. TCEP was removed and the protein was transferred to 50 mM NaH_2PO_4, 250 mM NaCl, 0.5 mM EDTA, 0.1% DDM pH 7 by four rounds of ultrafiltration in an Amicon Ultra-0.5 Centrifugal Filter Unit. Next, the concentrated (100 μM) bR solution was added to lyophilized maleimide-DNA oligonucleotide (1:2 bR:DNA) and incubated in darkness for 1.5 h. Subsequently, to remove excess DNA, the bR sample was bound to a Ni-NTA resin preequilibrated with 50 mM Tris 300 mM NaCl 0.5% DDM pH 7.5. The resin was then washed with 50 mM Tris 650 mM NaCl 0.5% DDM pH 7.5, and the sample was eluted with 50 mM Tris, 300 mM NaCl, 0.1% DDM, 500 mM imidazole, pH 7.5.

Next, the sample was transferred to 50 mM Tris 0.025% DDM 0.5 mM EDTA pH 7.5 and applied to an ion exchange Mono Q 5/50 GL column preequilibrated with the same buffer. The bR was separated from DNA-modified by applying a 1 M NaCl gradient over 40 column volumes. The peaks were analyzed using SDS-PAGE and the fractions containing DNA-bR were pooled and concentrated to approximately 30 μM to be used in ND assembly.

5.4 | ND Preparation

ND assembly was done as described previously [57]. Briefly, the lipid film containing DMPC or DMPC/Rhod-PE (98:2) was hydrated using 100 mM sodium cholate in 20 mM Tris 100 mM NaCl, 0.5 mM EDTA pH 7.5, with the final lipid concentration of 40 mM and vortexed until clear. Next, the MSP1E3D1(S22C, A157C) was added to the lipid mixture followed by an addition of bR or DNA-bR (for the bR-containing NDs) so that the final ratios were 1:150 MSP1E3D1S22C A157C:lipids for empty NDs and 1:5:750 bR:MSP1E3D1 S22C A157C:lipids for bR-loaded NDs. This was followed by addition of buffered 100 mM sodium cholate to bring the total concentration of sodium cholate to 28 mM. The final concentration of lipids in the sample was typically 6 mM.

ND assembly was initiated by the addition of 0.5 g/mL of activated Amberlite XAD-2 (Supelco) and incubation at 28°C for with 700 rpm shaking. After 3 h, Amberlite XAD-2 was replaced with a fresh portion (0.5 g/mL) of the resin and incubation continued for 1 h. Following this the samples were removed from the

resin. For-bR containing NDs, the empty NDs were removed by applying the samples to Ni-NTA resin preequilibrated with 50 mM Tris 300 mM NaCl pH 8.0 washing the resin with 50 mM Tris 300 mM NaCl 10 mM imidazole pH 8.0. The bR-containing NDs were eluted with 50 mM Tris 300 mM NaCl 500 mM imidazole pH 8.0. The prepared NDs were further purified and moved to the conjugation buffer (20 mM HEPES 400 mM KCl pH 7.2) using Superdex 200 Increase 10/300 GL (Cytiva).

5.5 | ND-DNA Conjugation

MSP1E3D1 $^{S22C\ A157C}$ NDs were reduced using immobilized TCEP disulfide reducing gel (Thermo Scientific), following the vendor's instructions for batch format reduction. Next, freshly reduced MSP1E3D1 S22C A157C NDs were mixed with 4x excess of lyophilized malemide-modified oligonucleotide over cysteines (8:1 maleimide-DNA:MSP1E3D1S22C A157C) in a buffer containing 25 mM HEPES 400 mM KCl pH 7.2. Total protein concentration was typically 50 μM and with total reaction volume being 100 μl. After mixing, reaction was incubated for 1 h at 25°C. Excess unreacted DNA was removed using Superdex 200 Increase 10/300 GL (Cytiva) preequilibrated with 20 mM HEPES 400 mM KCl pH 7.2.

5.6 | Scaffold DNA Production

The 3024 nt ssDNA scaffold for preparation of DNA origami was produced in-house following published protocol using pScaf-3024.1, a gift from Shawn Douglas [59] (Addgene plasmid #111404) as the scaffold template strand and helper plasmid for phagemid production—HP17_KO7, a gift from Hendrik Dietz [60] (Addgene plasmid #120346).

5.7 | DNA Ring Assembly and Purification

DNA origami rings were assembled by mixing 50 nM scaffold with 200 nM staples in assembly buffer containing 5 mM Tris, 1 mM EDTA, and 10 mM $MgCl_2$, pH 8. Structures were then annealed using the following temperature ramp: heating to 80°C for 5 min, then cooling from 60°C to 40°C, with a cooling ramp of −1°C/100 min followed by cooling from 40°C to 20°C with a cooling ramp of −1°C/10 min. To remove the excess of staples, the DNA origami solution was mixed with 2 volumes of PEG precipitation buffer containing 15% (w/v) PEG-8000 in 5 mM Tris 500 mM NaCl, 20 mM $MgCl_2$, pH 8. After mixing, samples were incubated for 30 min at room temperature and then centrifuged at 15,000 x *g* for 10 min. After careful removal of the supernatant, the DNA origami samples were resuspended in assembly buffer and incubated for 20 min at 37°C before estimating the concentration via UV–vis absorption.

5.8 | DNA ND Docking

10 nM DNA rings containing the chosen linker strands were mixed with purified NDs in a 1:3 ratio in 1 x assembly buffer and incubated for 30 min at 30°C. The sequenced docking experiments were performed by mixing the blocking strands with DNA ring in a 1:1 ratio followed by incubation for 30 min at 30°C. This was followed by the addition of DNA-modified-NDs containing DNA modified bR (1:3 DNA ring:ND ratio) and further incubation for 30 min at 30°C. Finally, the "release" strands were added to the sample at a 1:1 ratio, followed by final incubation for 30 min at 30°C.

5.9 | Ultracentrifugation of DOC-NDs

To separate the DOC-NDs from free NDs, ultracentrifugation in a glucose gradient was performed. Briefly, 400 μL layers of buffered 45%, 40%, 35%, 30%, 25%, 20%, and 15% glucose solution were carefully placed in an open-top thick-walled polycarbonate tube (3.5 mL, 13 × 51 mm; Beckman Coulter). Following this, 100 μL of the sample was applied on top of the gradient and the separation was done for 3 h at 268 000 g in a precooled (4°C) Optima MAX-XP (Beckman Coulter) centrifuge using a MSL-50 swinging bucket rotor. After the separation, 14 equal fractions were carefully collected from top to bottom using a micropipette and concentrated using 10 kDa cutoff Amicon filters.

5.10 | DLS

DLS experiments were done at 25°C using a Zetasizer NANO ZSP (Malvern) and disposable UV micro cuvettes.

5.11 | AFM Imaging

The AFM micrographs were acquired using a Bruker Dimension Icon microscope with Bruker ScanAsyst-Fluid+ probes (nominal spring constant equal to 0.7 N m^{-1}) in fluid mode. For imaging, the mica was freshly cleaved and 1.5 μL of 10 nM DNA origami sample was deposited followed by 1 min of incubation. Following this, 20 μL TAE with 12.5 mM $MgCl_2$ was added followed by the addition of 1.5 μL of 100 mM $NiCl_2$ and 1 min incubation. Finally, 140 μL of TAE with 12.5 mM $MgCl_2$ was added and sample was imaged.

5.12 | NS-TEM Imaging

For NS-TEM imaging, 5 μL of 10 nM origami sample was applied to Formvar/carbon-coated grids, 400 mesh copper grids (EM Resolutions) freshly glow discharged prior to sample deposition. After 1 min, the sample was blotted from the grid using filter paper and 5 μL of uranyl acetate (3%) was added to the grid. After 1 min, the grid was again blotted and left to dry for at least 1 h before imaging using a JEOL JEM-1230 microscope operated at 80 kV. Images were taken using a 4kx4k camera (TVIPS) equipped with EMMENU software ver. 4.0.9.87.

5.13 | Cryo-EM Imaging

For cryo-EM imaging, the samples were prepared by applying 3 μL of ∼40 nM DOC-ND sample to freshly glow discharged (Leica, 8 mA/60 sec) ultrathin carbon on lacey carbon (400 mesh) supported copper grids (Agar Scientific). The grids were plunge-frozen in liquid ethane using a Thermo FEI Vitrobot Mark IV using the following parameters: blot force 7, blot wait time 6, and waiting time 30 s, respectively. The temperature was set

to 10°C and the humidity to 100%. Data were collected on a Krios G3i microscope at the Polish National cryoEM Facility, SOLARIS, using a Gatan K3 camera with a Gatan BioQuantum energy filter operated with a slit width of 20 eV. Movies were collected at a 64 000× nominal magnification, resulting in a calibrated physical pixel size of 1.4 Å using EPU 2.10.0.1941REL. Movies were saved at physical pixel size as gain-corrected TIFF files. 3082 movies were collected with the range of defocus set −3.0, −2.7, −2.4, −2.1, −1.8, −1.5 µm and a total dose of 39.29 e/Å^2 over 40 frames. All processing was carried out in CryoSPARC v. 3.2.0 [61]. Movies were motion- and CTF-corrected in patch mode. Thumbnails of motion-corrected micrographs were used for visual analysis of DOC-ND loading as shown in Fig. S7. For 2D analysis, ND particles were picked with Topaz [62] (69 093 total) and particles with a single ND in different orientations were selected (17 935 total). Particles were then recentered and re-extracted with a larger 600 px box to accommodate the DNA ring.

15 247 particles were extracted and underwent further 2D classification. 48% of particles were attributed to the classes with DNA ring, and these classes were the largest ones (Fig. S8).

For tilt-series acquisition, the micrographs were collected at 53000x magnification in EFTEM mode using an energy filter with a 50 eV slit, with a pixel size 0.83 Å and a total dose of 100–150 e/Å^2. The tilted images were acquired in a range from −50° to 50° in 2° increments. The tomograms were prepared by processing using IMOD with patch-tracking mode used for fiducial model generation [63].

Author Contributions

Piotr Stepien: conceptualization (equal), formal analysis (lead), investigation (equal), methodology (equal), supervision (lead), validation (lead), visualization (lead), writing – original draft (lead), writing – review and editing (equal). **Gerrit Wilkens**: investigation (equal), methodology (equal), writing – original draft (supporting), writing – review and editing (supporting). **Sylwia Swiatek**: investigation (supporting), methodology (supporting). **Manuel Robles**: investigation (supporting), writing – original draft (supporting), writing – review and editing (supporting). **Anna Swietlikowska**: investigation (supporting), methodology (supporting). **Sarah Hutchings**: investigation (supporting). **Dmitry Ghilarov**: conceptualization (supporting), data curation (supporting), formal analysis (supporting), investigation (supporting), writing – original draft (supporting), writing – review and editing (supporting). **Jonathan Gardiner Heddle**: data curation (lead), funding acquisition (lead), investigation (supporting), methodology (supporting), project administration (lead), resources (lead), supervision (supporting), writing – original draft (supporting), writing – review and editing (equal).

Acknowledgments

We thank Olga Woźnicka for technical support with NS-TEM. We thank L. Koziej for support in cryo-EM measurements and tomographs analysis. We thank Y. Sakai for inspiring the DNA origami graphics in this article. Access to the KRIOS microscope at the National Synchrotron Radiation Centre SOLARIS is supported by the Ministry of Science and Higher Education, Poland, under contract no. 1/SOL/2021/2. We acknowledge the cryo-EM facility and staff at the SOLARIS National Synchrotron Radiation Centre, Poland. We thank M. Rawski and G. Ważny for their support with data collection. We thank the MCB Structural Biology Core Facility (supported by the TEAM TECH CORE FACILITY/2017-4/6 grant from the Foundation for Polish Science). We thank M.S. Islam for the help with acquiring the AFM data and Szczepan Zapotoczny for use of AFM equipment.

Funding

This study was supported by The Leverhulme Trust (grant LIP-2022-010), Fundacja na rzecz Nauki Polskiej (grant TEAM/2016-3/23), Wellcome Trust (grant 221868/Z/20/Z), and the Biotechnology and Biological Sciences Research Council (grant BB/X01097X/1). The authors acknowledge the support and the use of resources of Instruct-ERIC through the R&D pilot scheme APPID 3671.

Conflicts of Interest

The authors declare no conflicts of interest.

Data Availability Statement

Original data including raw gel images, data from AFM, NS-TEM, Cryo-EM, SDS PAGE, DLS, and agarose gels and chromatograms and photographs are deposited at Mendeley and are publicly available as of the date of publication (doi: 10.17632/5fxjdfpc22.1). All other data supporting the findings of this study are available from the corresponding authors upon reasonable request.

References

1. D. O. Daley, M. Rapp, E. Granseth, K. Melén, D. Drew, and G. von Heijne, "Global Topology Analysis of the E*scherichia Coli* Inner Membrane Proteome," *Science (1979)* 308, no. 5726 (2005): 1321–1323, https://doi.org/10.1126/science.1109730.

2. T. J. Stevens and I. T. Do Arkin, "More Complex Organisms Have a Greater Proportion of Membrane Proteins in Their Genomes?," *Proteins* 39, no. 4 (2000): 417–420, https://doi.org/10.1002/(sici)1097-0134(20000601)39:43.0.co;2-y.

3. A. Krogh, B. Larsson, G. von Heijne, and E. L. L. Sonnhammer, "Predicting transmembrane protein topology with a hidden markov model: application to complete genomes11Edited by F. Cohen," *Journal of Molecular Biology* 305, no. 3 (2001): 567–580, https://doi.org/10.1006/jmbi.2000.4315.

4. E. Wallin and G. Von Heijne, "Genome-Wide Analysis of Integral Membrane Proteins from Eubacterial, Archaean, and Eukaryotic Organisms," *Protein Science* 7, no. 4 (1998): 1029–1038, https://doi.org/10.1002/pro.5560070420.

5. J. P. Overington, B. Al-Lazikani, and A. L. Hopkins, "How Many Drug Targets Are There?," *Nature Reviews. Drug Discovery* 5, no. 12 (2006): 993–996, https://doi.org/10.1038/nrd2199.

6. H. Yin and A. D. Flynn, "Drugging Membrane Protein Interactions," *Annual Review of Biomedical Engineering* 18, no. 1 (2016): 51–76, https://doi.org/10.1146/annurev-bioeng-092115-025322.

7. S. Hirschi, T. R. Ward, W. P. Meier, D. J. Müller, and D. Fotiadis, "Synthetic Biology: Bottom-Up Assembly of Molecular Systems," *Chemical Reviews* 122, no. 21 (2022): 16294–16328, https://doi.org/10.1021/acs.chemrev.2c00339.

8. B. Sharma, H. Moghimianavval, S.-W. Hwang, and A. P. Liu, "Synthetic Cell as a Platform for Understanding Membrane-Membrane Interactions, *Membranes* 11, no. 12 (2021): 912, https://doi.org/10.3390/membranes11120912.

9. B. Ghosh, "Artificial Cell Design: Reconstructing Biology for Life Science Applications," *Emerging Topics in Life Sciences* 6, no. 6 (2022): 619–627, https://doi.org/10.1042/ETLS20220050.

10. I. G. Denisov, Y. V. Grinkova, A. A. Lazarides, and S. G. Sligar, "Directed Self-Assembly of Monodisperse Phospholipid Bilayer Nanodiscs with Controlled Size," *Journal of the American Chemical Society* 126, no. 11 (2004): 3477–3487, https://doi.org/10.1021/ja0393574.

11. S. G. Sligar and I. G. Denisov, "Nanodiscs: A Toolkit for Membrane Protein Science," *Protein Science* 30, no. 2 (2021): 297–315, https://doi.org/10.1002/pro.3994.

12. M. A. McLean, M. C. Gregory, and S. G. Sligar, "Nanodiscs: A Controlled Bilayer Surface for the Study of Membrane Proteins," *Annual Review of Biophysics* 47, no. 1 (2018): 107–124, https://doi.org/10.1146/annurev-biophys-070816-033620.

13. I. G. Denisov and S. G. Sligar, "Nanodiscs in Membrane Biochemistry and Biophysics," *Chemical Reviews* 117, no. 6 (2017): 4669–4713, https://doi.org/10.1021/acs.chemrev.6b00690.

14. D. M. Kern, B. Sorum, S. S. Mali, et al., "Structure of SARS-CoV-2 ORF3A in Lipid Nanodiscs," *Nature Structural & Molecular Biology* 28, no. 7 (2021): 573–582, https://doi.org/10.1038/s41594-021-00619-0.

15. M. Zhang, M. Gui, Z.-F. Wang, et al., "Structure of an Activated GPCR–G Protein Complex in Lipid Nanodiscs," *Nature Structural & Molecular Biology* 28, no. 3 (2021): 258–267, https://doi.org/10.1038/s41594-020-00554-6.

16. Y. Lee, T. Warne, R. Nehmé, et al., "Molecular Basis of β-Arrestin Coupling to Formoterol-Bound B1-Adrenoceptor," *Nature* 583, no. 7818 (2020): 862–866, https://doi.org/10.1038/s41586-020-2419-1.

17. W. Huang, M. Masureel, Q. Qu, et al., "Structure of the Neurotensin Receptor 1 in Complex with β-Arrestin 1," *Nature* 579, no. 7798 (2020): 303–308, https://doi.org/10.1038/s41586-020-1953-1.

18. D. P. Staus, H. Hu, M. J. Robertson, et al., "Structure of the M2 Muscarinic Receptor–β-Arrestin Complex in a Lipid Nanodisc," *Nature* 579, no. 7798 (2020): 297–302, https://doi.org/10.1038/s41586-020-1954-0.

19. D. Y. Zhao, M. Pöge, T. Morizumi, et al., "Structure of the Native Rhodopsin Dimer in Nanodiscs," *Journal of Biological Chemistry* 294, no. 39 (2019): 14215–14230, https://doi.org/10.1074/jbc.RA119.010089.

20. D. Ghilarov, S. Inaba-Inoue, P. Stepien, et al., "Molecular Mechanism of SbmA, a Promiscuous Transporter Exploited by Antimicrobial Peptides," *Science Advances* 7, no. 37 (2021): eabj5363, https://doi.org/10.1126/sciadv.abj5363.

21. N. T. Johansen, F. G. Tidemand, T. T. T. N. Nguyen, K. D. Rand, M. C. Pedersen, and L. Arleth, "Circularized and Solubility-Enhanced <scp>MSP</Scp> s Facilitate Simple and High-Yield Production of Stable Nanodiscs for Studies of Membrane Proteins in Solution," *FEBS Journal* 286, no. 9 (2019): 1734–1751, https://doi.org/10.1111/febs.14766.

22. M. L. Nasr, D. Baptista, M. Strauss, et al., "Covalently Circularized Nanodiscs for Studying Membrane Proteins and Viral Entry," *Nature Methods* 14, no. 1 (2017): 49–52, https://doi.org/10.1038/nmeth.4079.

23. N. T. Johansen, A. Luchini, F. G. Tidemand, et al., "Structural and Biophysical Properties of Supercharged and Circularized Nanodiscs," *Langmuir : the ACS Journal of Surfaces and Colloids* 37, no. 22 (2021): 6681–6690, https://doi.org/10.1021/acs.langmuir.1c00560.

24. S. Dey, C. Fan, K. V. Gothelf, et al., DNA Origami, *Nature Reviews Methods Primers* 1, no. 1 (2021): 13, https://doi.org/10.1038/s43586-020-00009-8.

25. P. W. K. Rothemund, "Folding DNA to Create Nanoscale Shapes and Patterns," *Nature* 440, no. 7082 (2006): 297–302, https://doi.org/10.1038/nature04586.

26. G. A. Knappe, E.-C. Wamhoff, and M. Functionalizing Bathe, "DNA Origami to Investigate and Interact with Biological Systems," *Nature Reviews. Materials* 8, no. 2 (2022): 123–138, https://doi.org/10.1038/s41578-022-00517-x.

27. J. Fu, Y. R. Yang, A. Johnson-Buck, et al., "Multi-Enzyme Complexes on DNA Scaffolds Capable of Substrate Channelling with an Artificial Swinging Arm," *Nature Nanotechnology* 9, no. 7 (2014): 531–536, https://doi.org/10.1038/nnano.2014.100.

28. Z. Zhang and E. R. Chapman, "Programmable Nanodisc Patterning by DNA Origami," *Nano Letters* 20, no. 8 (2020): 6032–6037, https://doi.org/10.1021/acs.nanolett.0c02048.

29. Z. Zhao, M. Zhang, J. M. Hogle, W. M. Shih, G. Wagner, and M. L. Nasr, "DNA-Corralled Nanodiscs for the Structural and Functional Characterization of Membrane Proteins and Viral Entry," *Journal of the American Chemical Society* 140, no. 34 (2018): 10639–10643, https://doi.org/10.1021/jacs.8b04638.

30. B. Augustyn, P. Stepien, C. Poojari, et al., "Cholesteryl Hemisuccinate Is Not a Good Replacement for Cholesterol in Lipid Nanodiscs," *Journal of Physical Chemistry. B* 123, no. 46 (2019): 9839–9845, https://doi.org/10.1021/acs.jpcb.9b07853.

31. C. Lin, S. D. Perrault, M. Kwak, F. Graf, and W. M. Shih, "Purification of DNA-Origami Nanostructures by Rate-Zonal Centrifugation," *Nucleic Acids Research* 41, no. 2 (2013): e40–e40, https://doi.org/10.1093/nar/gks1070.

32. M. Mandelkern, J. G. Elias, D. Eden, and D. M. Crothers, "The Dimensions of DNA in Solution," *Journal of Molecular Biology* 152, no. 1 (1981): 153–161, https://doi.org/10.1016/0022-2836(81)90099-1.

33. Q. Chi, G. Wang, and J. Jiang, "The Persistence Length and Length per Base of Single-Stranded DNA Obtained from Fluorescence Correlation Spectroscopy Measurements Using Mean Field Theory," *Physica A: Statistical Mechanics and Its Applications* 392, no. 5 (2013): 1072–1079, https://doi.org/10.1016/j.physa.2012.09.022.

34. K. Grushin, M. A. White, and S. Stoilova-McPhie, "Reversible Stacking of Lipid Nanodiscs for Structural Studies of Clotting Factors," *Nanotechnology Reviews* 6, no. 1 (2017): 139–148, https://doi.org/10.1515/ntrev-2016-0073.

35. C. Kielar, Y. Xin, B. Shen, et al., "On the Stability of DNA Origami Nanostructures in Low-Magnesium Buffers," *Angewandte Chemie International Edition* 57, no. 30 (2018): 9470–9474, https://doi.org/10.1002/anie.201802890.

36. B. Kumar, R. Zhu, L. Hebert, H. Jegerschöld, and C, "Method to Visualize and Analyze Membrane Interacting Proteins by Transmission Electron Microscopy," *Journal of Visualized Experiments*, 121 (2017): 55148.https://doi.org/10.3791/55148.

37. D. Salvador, M. Glavier, G. Schoehn, et al., "Minimal Nanodisc without Exogenous Lipids for Stabilizing Membrane Proteins in Detergent-Free Buffer," *Biochimica et Biophysica Acta (BBA) - Biomembranes* 1861, no. 4 (2019): 852–860, https://doi.org/10.1016/j.bbamem.2019.01.013.

38. R. Puthenveetil, K. Nguyen, and O. Vinogradova, "Nanodiscs and Solution NMR: Preparation, Application and Challenges," *Nanotechnology Reviews*6, no. 1 (2017): 111–125, https://doi.org/10.1515/ntrev-2016-0076.

39. T. K. Ritchie, Y. V. Grinkova, T. H. Bayburt, et al., "Reconstitution of Membrane Proteins in Phospholipid Bilayer Nanodiscs," *Methods in Enzymology* 464 (2009): 211–231, https://doi.org/10.1016/S0076-6879(09)64011-8.

40. Y. Xu, S. Jiang, C. R. Simmons, et al., "Tunable Nanoscale Cages from Self-Assembling DNA and Protein Building Blocks," *ACS Nano* 13, no. 3 (2019): 3545–3554, https://doi.org/10.1021/acsnano.8b09798.

41. S.-T. Wang, B. Minevich, J. Liu, et al., Designed and Biologically Active Protein Lattices, *Nature Communications* 12, no. 1 (2021): 3702, https://doi.org/10.1038/s41467-021-23966-4.

42. G. Kong, M. Xiong, L. Liu, et al., "DNA Origami-Based Protein Networks: From Basic Construction to Emerging Applications," *Chemical Society Reviews* 50, no. 3 (2021): 1846–1873, https://doi.org/10.1039/D0CS00255K.

43. A. Rajendran, M. Endo, Y. Katsuda, K. Hidaka, and H. Sugiyama, "Photo-Cross-Linking-Assisted Thermal Stability of DNA Origami Structures and Its Application for Higher-Temperature Self-Assembly," *Journal of the American Chemical Society* 133, no. 37 (2011): 14488–14491, https://doi.org/10.1021/ja204546h.

44. T. S. Young, I. Ahmad, J. A. Yin, and P. G. Schultz, "An Enhanced System for Unnatural Amino Acid Mutagenesis in E. coli," *Journal of Molecular Biology* 395, no. 2 (2010): 361–374, https://doi.org/10.1016/j.jmb.2009.10.030.

45. M. Synakewicz, D. Bauer, M. Rief, and L. S. Itzhaki, "Bioorthogonal Protein-DNA Conjugation Methods for Force Spectroscopy," *Scientific Reports* 9, no. 1 (2019): 13820, https://doi.org/10.1038/s41598-019-49843-1.

46. D. Zhao, Y. Kong, S. Zhao, and H. Xing, "Engineering Functional DNA–Protein Conjugates for Biosensing, Biomedical, and Nanoassembly Applications," *Topics in Current Chemistry* 378, no. 3 (2020): 41, https://doi.org/10.1007/s41061-020-00305-7.

47. J. B. Trads, T. Tørring, and K. V. Gothelf, "Site-Selective Conjugation of Native Proteins with DNA," *Accounts of Chemical Research* 50, no. 6 (2017): 1367–1374, https://doi.org/10.1021/acs.accounts.6b00618.

48. G. Bernardinelli and B. Högberg, "Entirely Enzymatic Nanofabrication of DNA–Protein Conjugates," *Nucleic Acids Research* 45, no. 18 (2017): e160–e160, https://doi.org/10.1093/nar/gkx707.

49. M. A. Koussa, M. Sotomayor, and W. P. Wong, "Protocol for Sortase-Mediated Construction of DNA–Protein Hybrids and Functional Nanostructures," *Methods* 67, no. 2 (2014): 134–141, https://doi.org/10.1016/j.ymeth.2014.02.020.

50. Y. Z. Tan, P. R. Baldwin, J. H. Davis, et al., "Addressing Preferred Specimen Orientation in Single-Particle Cryo-EM through Tilting," *Nature Methods* 14, no. 8 (2017): 793–796, https://doi.org/10.1038/nmeth.4347.

51. R. F. Thompson, M. Walker, C. A. Siebert, S. P. Muench, and N. A. Ranson, "An Introduction to Sample Preparation and Imaging by Cryo-Electron Microscopy for Structural Biology," *Methods* 100 (2016): 3–15, https://doi.org/10.1016/j.ymeth.2016.02.017.

52. K. Jahnke, N. Ritzmann, J. Fichtler, et al., Proton Gradients from Light-Harvesting E. Coli Control DNA Assemblies for Synthetic Cells, *Nature Communications* 12, no. 1 (2021): 3967, https://doi.org/10.1038/s41467-021-24103-x.

53. Y. Bogawat, S. Krishnan, F. C. Simmel, and I. Santiago, "Tunable 2D Diffusion of DNA Nanostructures on Lipid Membranes," *Biophysical Journal* 121, no. 24 (2022): 4810–4818, https://doi.org/10.1016/j.bpj.2022.10.015.

54. R. Rubio-Sánchez, S. E. Barker, M. Walczak, P. Cicuta, and L. D. Michele, "A Modular, Dynamic, DNA-Based Platform for Regulating Cargo Distribution and Transport between Lipid Domains," *Nano Letters* 21, no. 7 (2021): 2800–2808, https://doi.org/10.1021/acs.nanolett.0c04867.

55. Y. Suzuki, H. Sugiyama, and M. Endo, Complexing DNA Origami Frameworks through Sequential Self-Assembly Based on Directed Docking, *Angewandte Chemie International Edition* 57 (2018): 7061–7065, https://doi.org/10.1002/anie.201801983

56. X. Wang, H. Jun, and M. Bathe, "Programming 2D Supramolecular Assemblies with Wireframe DNA Origami," *Journal of the American Chemical Society* 144, no. 10 (2022): 4403–4409, https://doi.org/10.1021/jacs.1c11332.

57. P. Stępień, S. Świątek, M. Y. Y. Robles, et al., "CRAFTing Delivery of Membrane Proteins into Protocells Using Nanodiscs," *ACS Applied Materials & Interfaces*. (2023), https://doi.org/10.1021/acsami.3c11894.

58. I. G. Denisov, B. J. Baas, Y. V. Grinkova, and S. G. Sligar, "Cooperativity in Cytochrome P450 3A4," *Journal of Biological Chemistry* 282, no. 10 (2007): 7066–7076, https://doi.org/10.1074/jbc.M609589200.

59. P. M. Nafisi, T. Aksel, and S. M. Douglas, "Construction of a Novel Phagemid to Produce Custom DNA Origami Scaffolds, *Synthetic Biology* 3, no. 1 (2018): ysy015, https://doi.org/10.1093/synbio/ysy015.

60. F. Praetorius, B. Kick, K. L. Behler, M. N. Honemann, D. Weuster-Botz, and H. Dietz, Biotechnological Mass Production of DNA Origami, *Nature* 552, no. 7683 (2017): 84–87, https://doi.org/10.1038/nature24650.

61. A. Punjani, J. L. Rubinstein, D. J. Fleet, and M. A. Brubaker, "cryoSPARC: algorithms for rapid unsupervised cryo-EM structure determination," *Nature Methods* 14, no. 3 (2017): 290–296, https://doi.org/10.1038/nmeth.4169.

62. T. Bepler, A. Morin, M. Rapp, et al., "Positive-Unlabeled Convolutional Neural Networks for Particle Picking in Cryo-Electron Micrographs," *Nature Methods* 16, no. 11 (2019): 1153–1160, https://doi.org/10.1038/s41592-019-0575-8.

63. J. R. Kremer, D. N. Mastronarde, and McIntosh, Computer Visualization of Three-Dimensional Image Data Using IMOD, *Journal of Structural Biology* 116, no. 1 (1996): 71–76, https://doi.org/10.1006/jsbi.1996.0013.

Supporting Information

Additional supporting information can be found online in the Supporting Information section.